Computational Fluid Dynamics (CFD) Simulations of Taylor Bubbles in Vertical and Inclined Pipes with Upward and Downward Liquid Flow

Computational Fluid Dynamics (CFD) Simulations of Taylor Bubbles in Vertical and Inclined Pipes with Upward and Downward Liquid Flow

E. Lizarraga-Garcia, Projects & Technology, Shell Global Solutions (US) Inc., Department of Mechanical Engineering, MIT; J. Buongiorno, Department of Nuclear Science and Engineering, MIT; and E. Al-Safran, Department of Petroleum Engineering, Kuwait University

Corresponding Author: E. Lizarraga-Garcia
E-mail: elizaga@alum.mit.edu

Abstract

Two-phase flow is a common occurrence in pipes of oil and gas developments. Current predictive tools are based on the mechanistic two-fluid model, which requires the use of closure relations to predict integral flow parameters such as liquid holdup (or void fraction) and pressure gradient. However, these closure relations carry the highest uncertainties in the model. In particular, significant discrepancies have been found between experimental data and closure relations for the Taylor bubble velocity in slug flow, which has been determined to strongly affect the mechanistic model predictions (Lizarraga-García, 2016). In this work, we study the behavior of Taylor bubbles in vertical and inclined pipes with upward and downward flow using a validated 3D Computational Fluid Dynamics (CFD) approach with Level Set (LS) method implemented in a commercial code. A total of 56 cases are simulated covering a wide range of fluid properties, and pipe diameters and inclination angles ($Eo \in [10, 700]$, $Mo \in [1 \cdot 10^{-6}, 5 \cdot 10^{3}]$, $Re_{SL} \in [-40, 10]$, $\theta \in [5°, 90°]$). For bubbles in vertical upward flows, the simulated distribution parameter, C_0, is successfully compared with an existing model. However, the C_0 values of downward and inclined slug flows where the bubble becomes asymmetric are shown to be significantly different from their respective vertical upward flow ones, and no current model exists for the fluids simulated here. The main contributions of this work are (i) the relatively large 3D numerical database generated for this type of flow, (ii) the study of the asymmetric nature of inclined and some vertical downward slug flows, and (iii) the analysis of its impact on the distribution parameter, C_0.

Introduction

Two-phase slug flow is a common occurrence in wells, riser pipes and pipelines of crude oil and natural gas systems. Current predictive tools for two-phase flow are based on either the mixture model or the mechanistic two-fluid model (Brill and Mukherjee, 1999). In the latter, slug flow is modeled as a sequence of fundamental units, also called slug units. Each unit contains a long bullet-shaped bubble, known as Taylor bubble, and a liquid portion with smaller homogeneously distributed bubbles, known as liquid slug. Thorough studies about the modeling of two-phase slug flow can be found in Taitel and Barnea (1990); Fabre and Liné (1992); Bendiksen et al. (1996). The mechanistic model requires the use of closure relations to capture the transfer of mass, momentum and energy between the phases, in their respective conservation equations, so that integral flow parameters such as liquid holdup (or void fraction) and pressure gradient can be predicted. However, these closure relations typically carry the highest uncertainties in the model, since they are obtained empirically or through the use of overly simplified assumptions, and are applied beyond their range of applicability. In particular, significant discrepancies have been found between experimental data and closure relations for the Taylor bubble velocity in slug flow. For example, the drift velocity of Petalas and Aziz (2000) mechanistic model is predicted by the model of Bendiksen (1984) which was obtained based on air/water experiments; or the distribution parameter C_0 used by Gomez et al. (2000) is independent from inclination angle, and also based on the air/water experiments performed by Bendiksen (1984). Furthermore, the Taylor bubble velocity has been determined to strongly affect the pressure gradient and liquid holdup predicted by the mechanistic models of Ansari et al. (1994); Orell and Rembrand (1986); Petalas and Aziz (2000), as shown by Lizarraga-García (2016).

Taylor bubble velocity, v_{TB}, in slug flow is generally modeled based on the drift flux approach of Nicklin et al. (1962),

$$v_{TB} = C_0 \cdot v_m + v_d, \qquad [1]$$

where v_d is the *drift velocity* of the bubble in a stagnant liquid, and $C_0 \cdot v_m$ is the contribution of the *mixture velocity*, v_m, which is the sum of the liquid and gas superficial velocities, $v_m = v_{SL} + v_{Sg}$. The *distribution parameter*, C_0, is a dimensionless coefficient that captures the effect of nonuniform flow and void concentration profiles, and is generally approximated as the ratio of the maximum to the mean velocity in vertical pipes. Our previous published work focused on the Taylor bubble in stagnant liquid, i.e., the second term of the right hand side (RHS) of equation 1, v_d: in Lizarraga-Garcia et al. (2017), we proposed a new

E. Lizarraga-Garcia, Projects & Technology, Shell Global Solutions (US) Inc., Department of Mechanical Engineering, MIT; J. Buongiorno, Department of Nuclear Science and Engineering, MIT; and E. Al-Safran, Department of Petroleum Engineering, Kuwait University

Table 1 – Approximate Mo ranges for various oils based on British Petroleum (2011).

	ρ_L [kg/m^3]	σ [N/m]	μ_L [Pa·s]	Mo
Heavy oil	1100	0.03	2	$5{\cdot}10^{3}$
High viscous oil	1100	0.03	0.15	$2{\cdot}10^{-1}$
Medium viscous oil	1000	0.03	0.03	$3{\cdot}10^{-4}$
Light oil	900	0.03	0.007	$1{\cdot}10^{-6}$
Very light oil	800	0.03	0.001	$5{\cdot}10^{-10}$

closure relation for inclined pipes based on numerical results generated by the same approach followed in the present article, and whose higher accuracy compared to other literature correlations has been recently highlighted (Massoud, 2019; Mitchell, 2019; de Azevedo et al., 2020). The present manuscript investigates numerically the velocity and dynamics of Taylor bubbles in vertical and inclined pipes with imposed fluid flow, and analyzes the current prediction tools for C_0.

Taylor bubble's dynamics are influenced by the viscous, inertial, gravitational, and interfacial forces acting on it. If one assumes that the liquid transport properties are dominant ($\rho_g/\rho_L \ll 1$, $\mu_g/\mu_L \ll 1$, where the subscripts g and L indicate the gas and liquid phases, respectively, ρ is the density, and μ is the dynamic viscosity), dimensional analysis indicates the model of Nicklin et al. (1962) (equation 1) can be expressed as

$$Fr_{TB} = C_0(Eo, Mo, Re_{SL}, \theta)Fr_{SL} + Fr_d(Eo, Mo, \theta), \quad [2]$$

where Fr is the *Froude* number, $Fr = v/\sqrt{gd}$, where g is the gravitational acceleration and d is the pipe diameter; Eo is the *Eötvös* number, $Eo = \rho_L g d^2/\sigma$, where σ is the surface tension; Mo is the *Morton* number, $Mo = g\mu_L^4/\rho_L\sigma^3$; Re_{SL} is the liquid flow *Reynolds* number, $Re_{SL} = \rho_L v_{SL} d/\mu_L$; and θ is the pipe inclination angle measured from the horizontal. In this case, $v_m = v_{SL}$ since we only impose liquid flow in our simulations, as described later. Note that the choice of the *pi*-groups is not unique and the *inverse viscosity* number, N_f, a combination of both Eo and Mo, $N_f = (Eo^3/Mo)^{1/4}$, can also be employed.

Table 1 shows the approximate Mo ranges for different types of oil. In this work, we focus on $Mo \geq 1{\cdot}10^{-6}$ as ample work has been done using water, which has similar properties to very light oil.

In this manuscript, we first perform a literature review of the work centered on the first term of equation 1, i.e. the distribution parameter C_0 (for a more ample literature review on the study of Taylor bubbles in stagnant pipes, the interested reader is referred to Lizarraga-Garcia et al. (2017)). Then, we cover the mathematical model, test matrix and simulations setup, followed by the results and discussion. Finally, we present the conclusions.

Literature review

The literature on Taylor bubbles in vertical pipes with imposed fluid flow is ample. Shortly after Nicklin et al. (1962), Zuber and Findlay (1965) proposed a general expression for two-phase flow systems that took into account both the effect of nonuniform flow and void concentration profiles as well as the effect of local relative velocity between the phases. The authors defined the distribution parameter C_0 as

$$C_0 = \frac{\langle \alpha v_m \rangle}{\langle \alpha \rangle \langle v_m \rangle}, \quad [3]$$

where α is the local void fraction, and the operator $\langle x \rangle$ indicates the average value of a quantity x over the cross-sectional area of the pipe. In vertical slug flow, the Taylor bubble occupies almost the entire pipe thus $\langle \alpha \rangle \approx 1$. Furthermore, since the Taylor bubble occupies the center part of the pipe where the velocity is higher, $C_0 > 1$. Experiments with air/water (Nicklin et al., 1962; Bendiksen, 1984; Polonsky et al., 1999), theory (Collins et al., 1978; Bendiksen, 1985), and numerical simulations (Mao and Dukler, 1990, 1991) have shown that $C_0 \approx 2$ for laminar flow and $C_0 \approx 1.2$ for turbulent flow are good engineering

Table 2 – Distribution parameter C_0 correlations for Taylor bubbles in vertical pipes with upward flow.

Model	Correlation
Bendiksen (1985)	$C_0 = 2.29\left(1-\frac{20}{Eo}\left(1-e^{-0.0125Eo}\right)\right)$, for laminar flow [4a]
	$C_0 = \frac{\log Re_{SL}+0.309}{\log Re_{SL}-0.743}\left(1-\frac{2}{Eo}\left(3-e^{-0.025Eo}\log Re_{SL}\right)\right)$, for turbulent flow [4b]
Fréchou (1986)	$C_0 = 1.2+\frac{0.8}{1+1\cdot 10^{-8}Re_{SL}^{2.55}}$ [5]
Petalas and Aziz (2000)	$C_0{}^{a} = (1.64+0.12\sin\theta)\,Re_{SL}^{-0.031}$ [6]
Tomiyama et al. (2001)	$C_0 = 1.5-0.5e^{-4\cdot 10^{-4}Eo^{2.36}}$, for $Re_{SL}<2,000$ [7a]
	$C_0 = 1.18+0.32e^{1.7\cdot 10^{-3}(2,300-Re_{SL})}$, for $Re_{SL}>2,300$ [7b]
Rattner and Garimella (2015)	$C_0 = f_{LS}C_{0,LS}+(1-f_{LS})C_{0,Ca}$ [8a]
	$f_{LS} = \left(\frac{1}{1+4,840Re_{SL}^{-0.163}}\right)^{0.816/Eo}$ [8b]
	$C_{0,LS} = 1.20+\frac{1.09}{1+(Re_{SL}/805)^4}$ [8c]
	$C_{0,Ca} = \frac{1}{1-0.61Ca^{0.33}}$ [8d]

[a] Also applicable to inclined pipes

approximations for vertical upward flow. More detailed literature correlations for the distribution parameter, C_0, are shown in table 2. Bendiksen (1985) proposed two different correlations for upward vertical laminar and turbulent flow when $Eo > 40$. Fréchou (1986) provided a correlation dependent only on Re_{SL}. Later, in his mechanistic model, Petalas and Aziz (2000) used a correlation that could also be applied to inclined pipes, which depends on both Re_{SL} and θ. Unfortunately, no details about the correlation derivation were included. Shortly after, and based on air/water experiments, Tomiyama et al. (2001) presented two correlations for laminar and turbulent flow, however the authors mentioned that the laminar expression is preliminary due to lack of sufficient experimental data. Finally, and using also air/water as the fluids, Rattner and Garimella (2015) studied experimentally the so-called *intermediate scale Taylor flow* (defined as $5 \leq Eo \leq 40$), for ranges $480 \leq Re_{SL} \leq 4,460$ and $4.9 \leq Eo \leq 12.2$ in upward vertical pipes. The authors proposed a blended capillary-to-large scale distribution parameter, C_0, for this transitional regime with two contributions: the large scale, $C_{0,LS}$, and the capillary scale, $C_{0,Ca}$, where the latter is obtained from Liu et al. (2005), and $Ca = \mu_L v_{SL}/\sigma$. The two contributions are combined with a large scale fraction function, f_{LS}, equation 8b.

Published research on vertical downward flow is more limited. In general, if the bubble remains axisymmetric, its velocity follows equation 1 with the value of C_0 being that of the upward flow for the same liquid and regime (Martin, 1976; Figueroa-Espinoza and Fabre, 2011; Fershtman et al., 2017). However, several experimental studies observed that in some downward flow cases the bubble nose begins to distort and the bubble becomes asymmetric (Griffith and Wallis, 1961; Nicklin et al., 1962; Polonsky et al., 1999).

In those cases, the value of C_0 is lower than unity. Martin (1976) performed a comprehensive study focused on downward water flow for three different pipe diameters (estimated $Eo = 92; 1,410; 2,670$), and obtained $C_0 < 1$ for the asymmetric bubble cases. The first attempt to theoretically analyzed this problem was done by Lu and Prosperetti (2006), who performed an approximate linear stability analysis neglecting surface tension effects, and "found that the major factor underlying the instability is the flattening of the bubble nose as the liquid flows downward". The authors proposed a critical downward liquid velocity, $Fr_{SL} \approx -0.135$, at which the bubble loses the symmetric shape. These authors published later a computational study of 2D axisymmetric Taylor bubbles in vertical pipes with upward and downward liquid flow where they also proposed an approximate criterion for the bubble tail shape (Lu and Prosperetti, 2009). Figueroa-Espinoza and Fabre (2011) studied through 2D channel simulations the transition from an axisymmetric to an asymmetric bubble shape in downward laminar liquid flow, and proposed a critical liquid velocity dependent on surface tension. Later, these authors also performed Taylor bubble experiments in a vertical pipe with downward flow (Fabre and Figueroa-Espinoza, 2014). They proposed a new critical velocity criterion based on the *vorticity-to-radius ratio* of the liquid on the pipe axis, $(\omega/r)_0$, and dependent again on surface tension. Fershtman et al. (2017) studied experimentally the Taylor bubble motion in vertical downward water flow and identified three distinct modes of bubble motion for downward liquid velocities exceeding $Fr_{SL} = -0.13$, which corresponds to the criterion of Lu and Prosperetti (2006).

Literature of Taylor bubbles in inclined pipes with imposed flow is somehow more scarce. Bendiksen (1984) included inclined upward and downward water flow experiments ($\theta = 90°$ to $-30°$), and reported $C_0 \in [1.00, 1.20]$ for all upward flow inclinations, and $C_0 < 1$ for downward flow. Roumazeilles et al. (1996) performed experiments of air/kerosene downward turbulent slug flow for those same inclination angles ($\theta = 0°$ to $-30°$), and reported that the Taylor bubble velocity was not affected by the inclination angle in their experiments yielding $C_0 \approx 1.2$. Ha-Ngoc and Fabre (2004) provided analytical and numerical solutions for the velocity and shape of 2D long bubbles, both plane and axisymmetric, for upward inclined flow. As pointed out by Taha and Cui (2006), "the difficulty in handling the 3D nature of the flow limits the existence of experimental data", as the axisymmetry of slug flow is breached when the tube is tilted away from the vertical. The authors simulated an air/water system with diameter $d = 0.2$ m ($Eo = 55$) using Volume of Fluid (VOF) as the interface tracking method for a number of upward flow vertical cases, and provided a feasibility case study for one inclined pipe example. Later, Hua et al. (2012) used Fluent (VOF) to study water and SF_6 fluids in inclined pipes for $Eo = 1,350$ and $1 \cdot 10^4 \leq Re_{SL} \leq 3 \cdot 10^5$.

The present work attempts to shed some light in the 3D nature of Taylor bubbles in vertical and inclined pipes with upward and downward flow through 3D CFD simulations of a wide range of fluid properties, and pipe diameters and inclination angles ($Eo \in [10, 700]$, $Mo \in [1 \cdot 10^{-6}, 5 \cdot 10^3]$, $Re_{SL} \in [-40, 10]$, $\theta \in [5°, 90°]$). The main focus of this work is to analyze the effect of those parameters on the distribution parameter, C_0, in order to predict the Taylor bubble velocity, which strongly affects the pressure gradient and liquid holdup prediction of mechanistic models (Lizarraga-García, 2016). Results highlight the need for improvement of the current models for inclined and downward slug flows where the axisymmetry is lost for fluids relevant to oil and gas systems. It should be stressed the numerical complexity of Taylor bubble 3D CFD simulations. This study presents, to the best of our knowledge, the first published numerical simulations for vertical downward flows where the 3D Taylor bubble becomes asymmetric.

CFD simulations

Mathematical model. Three dimensional CFD Direct Numerical Simulations (DNS) are performed with the CFD code TransAT® (2014), a finite-volume software developed at ASCOMP. The code uses structured meshes and *Message Passing Interface* (MPI) parallel-based algorithm to solve multi-fluid Navier-Stokes equations. Computer resources for this work include the supercomputers Titan and Eos of the Oak Ridge Leadership Computing Facility at the Oak Ridge National Laboratory.

The code uses the one-fluid formulation approach, where the flow is described by one fluid with variable material properties, which vary according to a color function advected by the flow. In the absence of phase

change phenomena, the mass and momentum conservation equations are

$$\frac{\partial \rho}{\partial t} + \nabla \cdot (\rho \mathbf{v}) = 0 \quad [9a]$$

$$\frac{\partial (\rho \mathbf{v})}{\partial t} + \nabla \cdot (\rho \mathbf{v}\mathbf{v}) = -\nabla p + \nabla \cdot \overline{\overline{\sigma}} + \rho \mathbf{g} + \mathbf{F}_s, \quad [9b]$$

where t is the time, $\mathbf{v}$ is the velocity vector, p is the pressure, $\overline{\overline{\sigma}} = \mu(\nabla \mathbf{v} + \nabla^T \mathbf{v})$ is the viscous stress tensor, $\mathbf{g}$ is the gravity vector, and $\mathbf{F}_s = \sigma \kappa \mathbf{n} \delta(\phi)$ is the surface tension term where $\kappa = \nabla \cdot (\nabla \phi / |\nabla \phi|)$ is the surface curvature, $\mathbf{n}$ is the vector normal to the interface, and δ is a smoothed delta function centered at the interface. In this work, the color function used is based on the Level Set (LS) method (Osher and Sethian, 1988; Sussman et al., 1994), where the interface is represented by a continuous and monotonous function ϕ that represents the distance to the interface at $\phi = 0$. The LS advection equation is given by

$$\frac{\partial \phi}{\partial t} + \mathbf{v} \cdot \nabla \phi = 0, \quad [10]$$

and material properties such as density and viscosity are updated locally based on ϕ, and smoothed across the interface using a smooth Heaviside function. Furthermore, the pipe is modeled as an embedded surface and represented in the fluid by the so-called Solid Level Set function $\phi_s = 0$, i.e. the Immersed Surfaces Technology (IST) technique (Chung, 2001; Labois et al., 2010). The mesh is locally refined near the pipe walls.

Simulations are carried out using the 2nd-order *Hybrid Linear/Parabolic Approximation* (HLPA) scheme (Zhu, 1991) for the discretization of the convective fluxes. An implicit 1st-order scheme is used for the time marching, where the time-step is adaptive and bounded by a Courant number fixed between 0.5 and 0.9 to guarantee stability of the simulations. The SIMPLEC (*Semi-Implicit Method for Pressure Linked Equations-Consistent*) algorithm is used for the pressure-velocity coupling (Doormaal and Raithby, 1984). For the LS, a 3rd-order *Weighted Essentially Non-Oscillatory* (WENO) scheme is used for re-distancing, and mass conservation is enforced using global and local mass-conservation schemes (Lakehal et al., 2002). Finally, the solvers used depend on the simulation. For high viscosity cases where the Navier-Stokes equations tend to elliptic, the R-cycle adaptive *Algebraic Multigrid* (AMG) method is used (R-cycle, 2016). Otherwise, either the incomplete lower-upper decomposition method *Strongly Implicit Procedure* (SIP) (Stone, 1968) or the *Generalized Minimum Residual* method (GMRES) (Saad and Schultz, 1986) are used, the latter with *hypre* AMG preconditioning (Falgout et al., 2006) of the parallel PETSc (*Portable, Extensible Toolkit for Scientific Computation*) library (Balay et al., 1997).

The code has been validated using in-house and literature experimental data for the Taylor bubble terminal velocities and bubble shapes in vertical and inclined pipes, and velocity vectors in vertical pipes. Those results are reported in Lizarraga-Garcia et al. (2017) and more details can be found in Lizarraga-Garcia et al. (2015); Lizarraga-García (2016).

Test matrix and simulations setup. In the present work, we simulate individual Taylor bubbles in pipes with imposed fluid flow. We study different fluid properties and pipe geometries, corresponding to the seven cases located in figure 1 and summarized in table 3. These are based on the database generated for Taylor bubble in stagnant liquid described in Lizarraga-Garcia et al. (2017), and cover an ample range of fluid properties and pipe geometries. For cases 1 to 7 of figure 1, upward and downward vertical flows are simulated. Moreover, for cases 5 to 7, upward and downward inclined flow are also studied for two additional inclination angles: $\theta = 45°, 5°$. Note that equation 2 can also be written using the liquid flow *Reynolds* number, Re_{SL}, as

$$Fr_{TB} = C_0 \frac{Re_{SL}}{N_f} + Fr_d. \quad [11]$$

Re_{SL} is the parameter included in table 3, where positive value means upward flow, and negative value means downward flow. A total of 56 cases are simulated.

Table 3 – Test matrix for simulations of Taylor bubble motion in pipes with imposed liquid flow.

Case	Eo	Mo	N_f	Re_{SL}	θ (°)
1	10	$1{\cdot}10^{-6}$	178	10, 1, 0, -1	90
2	10	$7.07{\cdot}10^{-2}$	10.9	10, 1, 0	90
3	28.9	$5{\cdot}10^{3}$	1.48	0.1, 0, -0.1	90
4	83.7	18.8	13.3	10, 1, 0, -1	90
5	28.9	$7.07{\cdot}10^{-2}$	24.2	10, 1, 0, -1, -10	90, 45, 5
6	242	$7.07{\cdot}10^{-2}$	119	10, 1, 0, -1, -10, -40	90, 45, 5
7	700	$5{\cdot}10^{3}$	16.2	1, 0, -1	90, 45, 5

The simulations start with a single bubble in still liquid and finish when the bubble reaches its terminal velocity. The bubble is placed inside a pipe with both ends open and embedded in the numerical domain. The boundary conditions of the numerical domain are an inflow plane at the pipe inlet, an outflow plane at the pipe outlet, and symmetry planes at the other four planes parallel to the pipe longitudinal axis. At the inflow plane, the velocity is set to a transient profile that evolves from zero at the simulation start to the Hagen-Poiseuille profile. At the outflow plane, the stream-wise gradients of all variables are set to zero, that is, fully developed flow condition. Finally, at the symmetry planes, the normal velocity and pressure gradient components are set to zero. The no-slip condition at the wall is imposed through a relaxation term which acts as a distributed momentum sink reducing the fluid velocity as the indicator function goes to zero (Beckermann et al., 1999). The structured mesh size is dependent on the case study and is refined until the terminal velocity converges. In order to capture the Kolmogorov scale, η, estimated as $\eta \sim d \cdot Re_{TB}^{-3/4}$, cell sizes used are smaller than those estimates. Re_{TB} magnitude ranges from 0.1 to 60, and thus the Kolmogorov scale, η, from 0.1 to 0.001 m. Number of cells ranges from 1 million up to 6.5 million, with mesh refinement at the pipe wall and a maximum cell aspect ratio of 3.

Finally, the results are analyzed based on two validated assumptions: the Taylor bubble length does not affect its rising velocity, and there exists a lubricating film between the Taylor bubble and the pipe wall at all inclinations. The first assumption is confirmed by simulating different bubble volumes for several cases, and is consistent with what has been widely reported in the literature (e.g. Tomiyama et al. (2001); Taha and Cui (2006); Lizarraga-Garcia et al. (2017)). Furthermore, the length of the bubbles simulated is well below the critical length required for the liquid film to drain and breakup based on the criterion proposed by Lizarraga-Garcia et al. (2016).

Results and discussion

In this section, we first present and discuss the results for vertical pipes for both upward and downward flow. Then, we cover the inclined pipe cases. The entire set of results are captured in table 6 of the appendix.

Vertical pipes. Figure 2 shows representative results from the three dimensional simulations. There, the numerically obtained Taylor bubble shapes and liquid streamlines for case 4 with imposed flow of $Re_{SL} = 1$ and $Re_{SL} = -1$, and case 6 with imposed flow of $Re_{SL} = 10$ and $Re_{SL} = -40$, respectively, are depicted. It can be observed that the Taylor bubble remains axisymmetric for the upward flow cases, whereas it becomes asymmetric for the downward flow cases. This phenomenon is further discussed later in the section.

First, the numerical results of Taylor bubble velocity in vertical pipes with upward flow are compared with the literature correlations of table 2. The parameters used for that comparison are the absolute average relative error, AAR, and the coefficient of determination, R^2, respectively defined as

$$AAR = \left(\frac{1}{N} \sum_{i}^{N} \frac{|C_{0,pred,i} - C_{0,CFD,i}|}{C_{0,CFD,i}} \right) \cdot 100, \qquad [12]$$

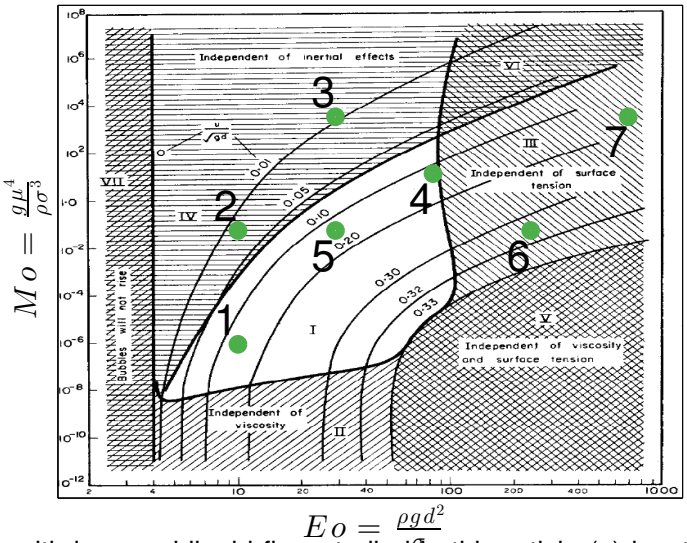

Fig. 1 – Numerical cases with imposed liquid flow studied in this article (•) located in the map of White and Beardmore (1962).

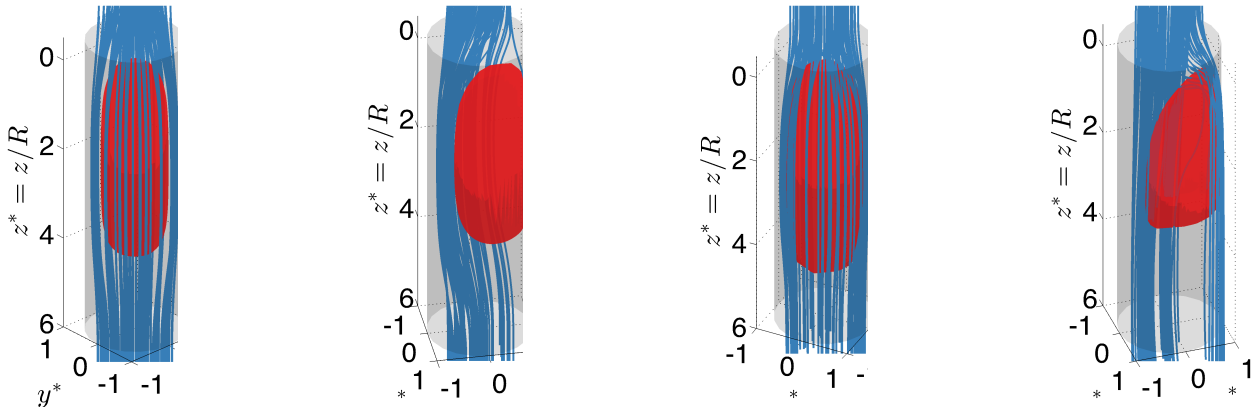

(a) (b) (c) (d)

Fig. 2 – Three dimensional Taylor bubble shape and liquid streamlines in vertical pipes for case 4 with imposed flow of $Re_{SL} = 1$ (a) and $Re_{SL} = -1$ (b), and case 6 with imposed flow of $Re_{SL} = 10$ (c) and $Re_{SL} = -40$ (d).

Table 4 – Upward vertical flow simulations comparison with respect to the literature correlations from table 2: absolute average relative error, AAR, and determination coefficient, R^2.

	Rattner and Garimella (2015)	Bendiksen (1985)	Fréchou (1986)	Petalas and Aziz (2000)	Tomiyama et al. (2001)
AAR	9.0	17	16	22	36
R^2	0.66	-0.043	-0.055	-0.97	-4.4

where N is the number of points, $C_{0,pred,i}$ is the predicted C_0 value of case i using a correlation, and $C_{0,CFD,i}$ is the numerically obtained C_0 value of case i, and

$$R^2 = 1 - \frac{\sum_i^N \left(C_{0,CFD,i} - C_{0,pred,i}\right)^2}{\sum_i^N \left(C_{0,CFD,i} - \overline{C}_{0,CFD}\right)^2}, \quad [13]$$

where the numerator is the sum of squares of the residuals, the denominator is the total sum of squares which is proportional to the variance of the data, and $\overline{C}_{0,sim}$ is the mean of the simulated results, $\overline{C}_{0,CFD} = \sum_i^N C_{0,CFD,i}/N$.

Table 4 shows the comparison results. It can be observed that the correlation from Rattner and Garimella (2015) (equations 8) provides the best fit. It should be highlighted again that Bendiksen (1985)'s model was developed for $Eo > 40$, and that Tomiyama et al. (2001) mentioned that the laminar expression is preliminary due to lack of sufficient experimental data. The purpose of the present comparison is to evaluate the predictions of current published correlations for the cases analyzed in this manuscript, not a comprehensive model performance study. Figure 3 shows those $C_{0,CFD}$ simulation results against Rattner and Garimella (2015)'s model predictions. The majority of the results shows an difference lower than 10%, with all results lying within the 25% difference bandwidth. The standard error of the calculated $C_{0,CFD}$, included in the figure bars, is obtained based on equation 2, i.e.,

$$\sigma_{C_{0,CFD}} = \sqrt{\sigma_{Fr_{TB}}^2 + \sigma_{Fr_d}^2} \Big/ |Fr_{SL}|, \quad [14]$$

where $\sigma_{Fr_{TB}}$ and σ_{Fr_d} are the standard errors of the numerically obtained Fr_{TB} and Fr_d, respectively, associated with the mesh convergence criterion used in the study: less than 1% relative error. Thus, as an estimate, we use $2\sigma_{Fr_{TB}} = 0.01 Fr_{TB}$ and $2\sigma_{Fr_d} = 0.01 Fr_d$. As shown in Figure 3, the estimated numerical error is relatively low. The two cases with the larger standard error correspond to relative low imposed Fr_{SL} where the difference between the simulated Fr_{TB} and Fr_d is correspondingly low.

In the case of downward flow, as explained in section , the situation can be more complex due to bubble instabilities that break the symmetry. Figure 4a shows the Fr_{TB} against the downward imposed flow, Fr_{SL}, for the simulated cases. The solid lines are obtained based on the mean value of C_0 for the corresponding upward flow cases, which would approximately predict the C_0 values for downward flows if the bubble would remain axisymmetric (e.g. figure 6c of Figueroa-Espinoza and Fabre (2011) or figure 2 of Fershtman et al. (2017)). The shaded areas of the figure correspond to the 95% confidence intervals based on the estimated error of the mean. Figure 4b compares the simulated $C_{0,CFD}$ versus those C_0 values. In general terms, it can be observed that the simulated Fr_{TB} follow the lines and that $C_{0,CFD}$ could be approximated by the corresponding case for upward flow. However, the three cases circled in red are clear outliers. In these cases, the Taylor bubble becomes asymmetric, as shown in figures 2 and 5, with its tip moving closer to the wall where the absolute liquid velocity is lower. That results in a significant lower C_0 value than for an axisymmetric bubble. What drives that phenomenon?

Figure 5 shows the Taylor bubble nose shape for all the vertical cases, where its dependence on the imposed flow, Re_{SL}, can be observed. For the upward flow cases ($Re_{SL} > 0$), the bubble shape becomes more pointed as the imposed fluid flow increases. For downward flow ($Re_{SL} < 0$), the behavior is slightly more intricate. On the one hand, for some cases (cases 1, 5), the bubble remains axisymmetric as the

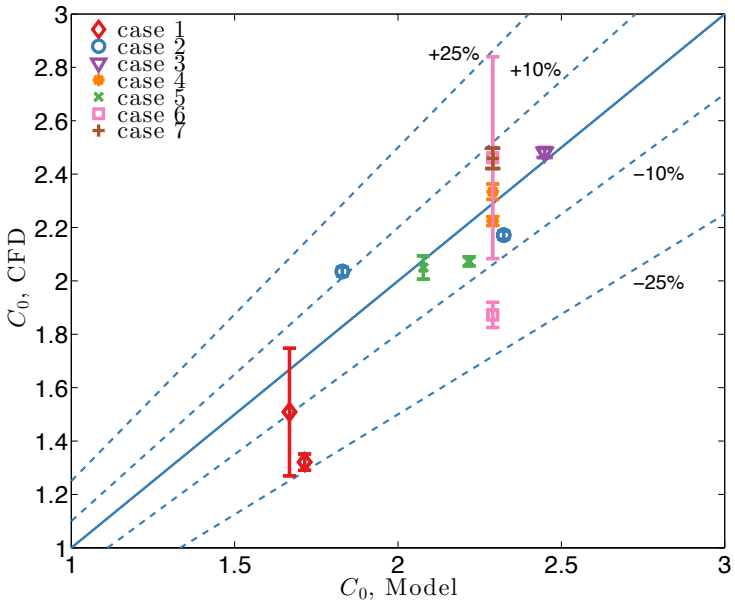

Fig. 3 – C_0 simulation results for vertical upward flow compared with predictions of Rattner and Garimella (2015)'s model.

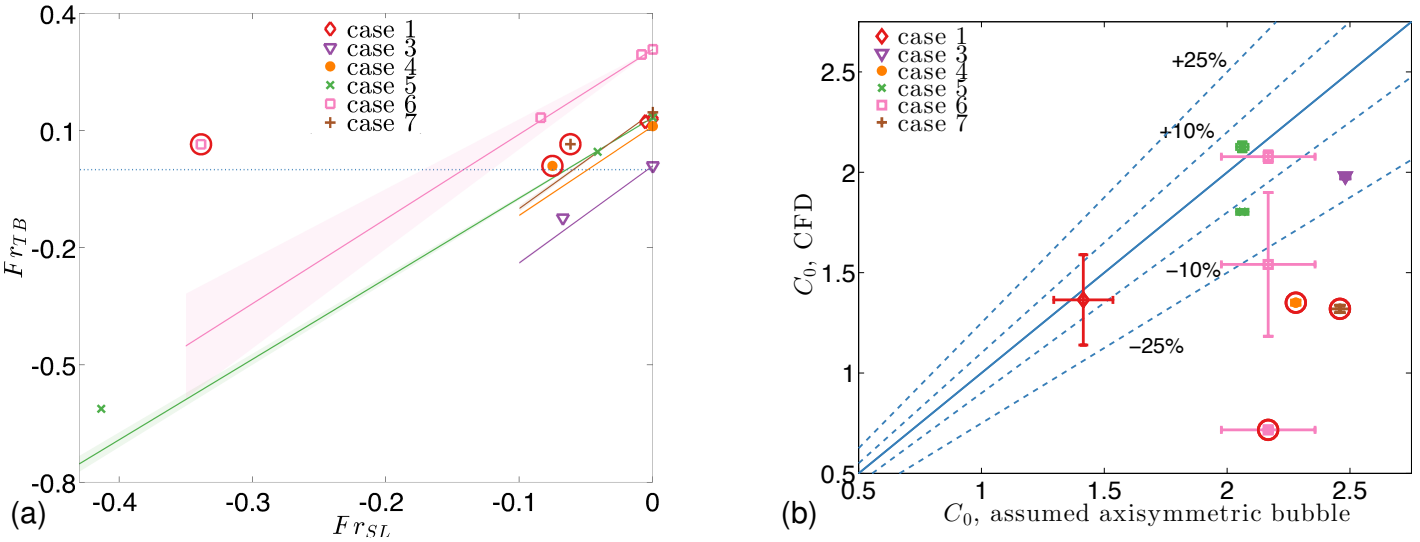

Fig. 4 – Downward flow cases in vertical pipes: simulated Fr_{TB} against the downward imposed flow, Fr_{SL}, where solid lines are based on the mean value of C_0 for the corresponding upward flow cases (a); and comparison of the simulated $C_{0,CFD}$ versus those C_0 values (b). Red circled cases (o) correspond to asymmetric bubble results.

Table 5 – Conditions at symmetry breaking for the present simulations.

Case	Eo	Σ	Mo	N_f	$-\Omega^*_{0,c,\text{i,min}}$	$-\Omega^*_{0,c,\text{i,max}}$
1	10	0.4	$1{\cdot}10^{-6}$	178	0.022	na
3	28.9	0.138	$5{\cdot}10^{3}$	1.48	0.27	na
4	83.7	0.0478	18.8	13.3	0	0.30
5	28.9	0.138	$7.07{\cdot}10^{-2}$	24.2	1.6	na
6	242	0.0165	$7.07{\cdot}10^{-2}$	119	0.34	1.4
7	700	0.00571	$5{\cdot}10^{3}$	16.2	0	0.25

downward liquid flow increases in absolute value. On the other hand, for the three cases mentioned above (cases 4, 6, 7), the bubble becomes asymmetric. In case 6, the bubble nose flattens as the downward flow increases until it becomes asymmetric. This would confirm the finding of Lu and Prosperetti (2006): the major factor underlying the bubble instability in vertical downward flows is the flattening of the bubble nose as the liquid flows downward. To the best of our knowledge, this is the first time this phenomenon has been observed in 3D numerical simulations. It is worth noting that the same asymmetric bubble shape is obtained for different bubble initial conditions in the three cases, thus confirming the stability of that solution.

We now analyze the transition liquid flow at which the symmetry is broken. In order to compare them to literature values, we use the *vorticity-to-radius ratio* of the liquid on the pipe axis, $-\Omega_0 = (\omega/r)_0$, based on Fabre and Figueroa-Espinoza (2014). For laminar flows, its nondimensional value is $\Omega^*_0 = 2Fr_0$, where Fr_0 is the *Froude* number of the liquid on the pipe axis, $Fr_0 = v_0/\sqrt{gd}$. I.e., $\Omega^*_0 = 4Fr_{SL}$. Our simulations are performed at limited imposed flow values, thus we provide a range of critical vorticity-to-radius ratios, $[-\Omega^*_{0,c,\text{i,min}},\ -\Omega^*_{0,c,\text{i,max}}]$, for each case $i = 1, 3, 4, 5, 6, 7$, shown in table 5. Note that $-\Omega^*_{0,c,\text{i,max}} = na$ denotes that the asymmetric bubble is not obtained in the simulations performed. In the literature, Griffith and Wallis (1961) measured the instability onset for water in three pipe diameters. The theoretical study of Lu and Prosperetti (2006), which neglected surface tension, proposed a critical downward liquid velocity $Fr_{SL} \approx -0.135$, i.e., $-\Omega^*_{0,c} \approx 0.54$. Fabre and Figueroa-Espinoza (2014) studied experimentally four laminar flow cases, and also proposed a critical $\Omega^*_{0,c}$ dependent linearly on the surface tension parameter, Σ,

$$\Omega^*_{0,c} = -(7.5\Sigma + 0.06) \pm 0.07, \qquad [15]$$

where Σ is an inverse *Eötvös* number, $\Sigma = 4\sigma/\rho_L g d^2 = 4/Eo$.

Figure 6 depicts the present and literature results. It shows that the predicted value of Lu and Prosperetti (2006) is a good initial attempt to theoretically study these instabilities. In general, it is observed that the critical $-\Omega^*_{0,c}$ increases with Σ (decreases with Eo). That is, for the same fluid, as the pipe diameter decreases, the instability onset requires higher downward liquid velocities due to surface tension effects increasing and preventing the bubble deformation. E.g. for cases 5 and 6, which have the same Mo number but $\Sigma_5 > \Sigma_6$, $-\Omega^*_{0,c,5} > -\Omega^*_{0,c,6}$. This trend is captured by equation 15. Furthermore, case 7 results also fall within the equation range prediction. However, the equation does not completely capture some of the results. For example, $-\Omega^*_{0,c,6} > -\Omega^*_{0,c,4}$ even though $\Sigma_6 < \Sigma_4$, and $-\Omega^*_{0,c,5}$ is also well outside the equation ranges. This suggests that viscosity may also have an effect in the instability, and that more work is required to further understand this phenomenon. It should be noted that the literature studies are based on relatively low viscosity fluids like water, with $Mo \in [1 \cdot 10^{-11}, 1 \cdot 10^{-8}]$. That is outside the Mo range of the liquids studied here, $Mo \in [1 \cdot 10^{-6}, 5 \cdot 10^{3}]$, thus reinforcing the need for further work with liquids more relevant to oil and gas systems. Finally, it should also be mentioned that case 1 is not included in figure 6. Σ_1 is relatively high, which would require the corresponding high downward liquid flows to be able to flatten the bubble and initiate the instability. However, the imposed flows simulated here barely deform the bubble, as shown in figure 5a, and $-\Omega^*_{0,c,1,\text{min}}$ is too low to represent a meaningful lower bound.

Finally, we analyze the bubble tail shape, as it has a strong impact on the wake. For example, figure 7

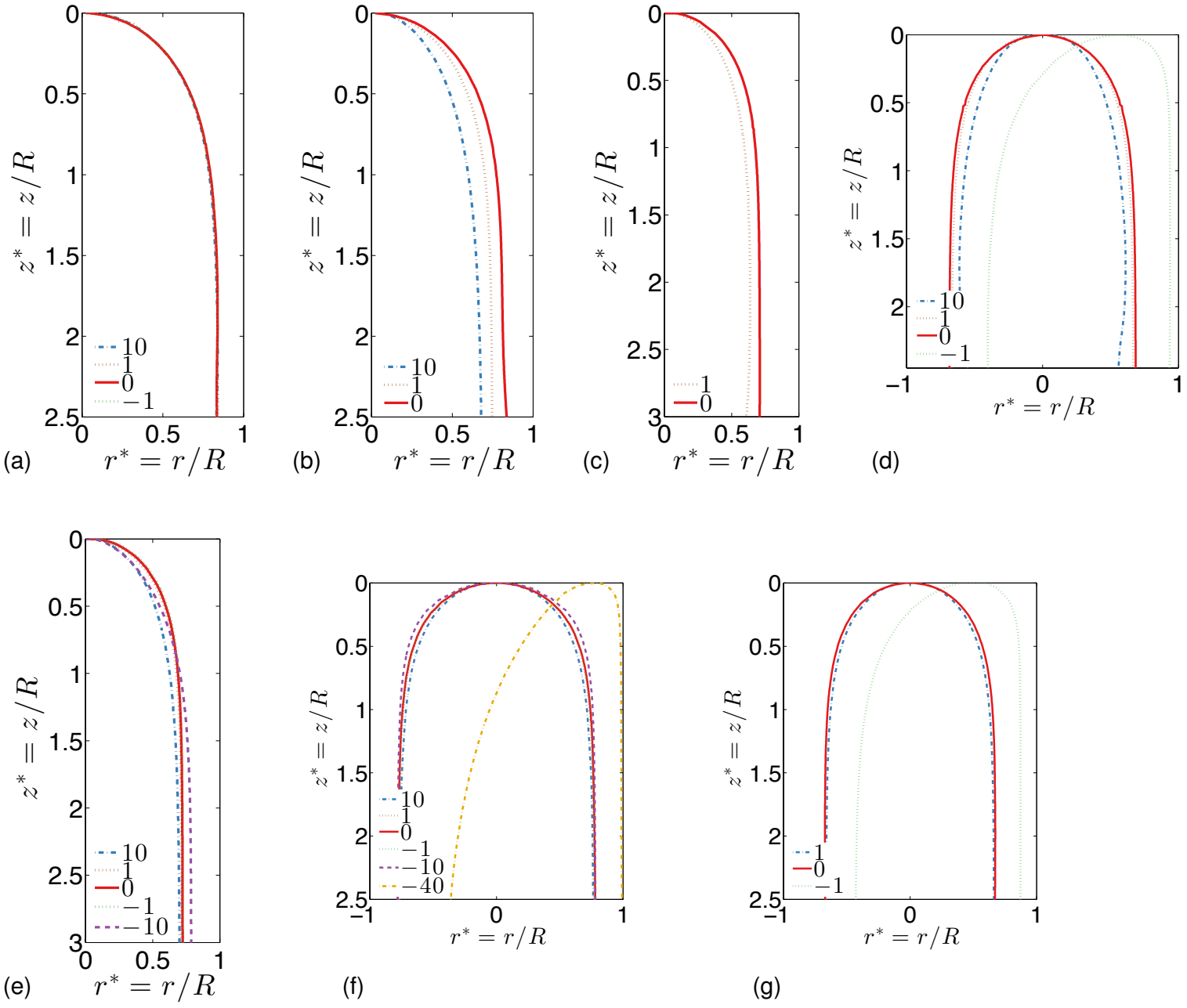

Fig. 5 – Taylor bubble shape dependence on fluid flow in vertical pipes ($\theta = 90°$) for cases 1 (a), 2 (b), 3 (c), 4 (d), 5 (e), 6 (f) and 7 (h). The legend numbers correspond to the imposed flow Re_{SL}, where $Re_{SL} > 0$ is upward flow, and $Re_{SL} < 0$ is downward flow.

E. Lizarraga-Garcia, Projects & Technology, Shell Global Solutions (US) Inc., Department of Mechanical Engineering, MIT; J. Buongiorno, Department of Nuclear Science and Engineering, MIT; and E. Al-Safran, Department of Petroleum Engineering, Kuwait University

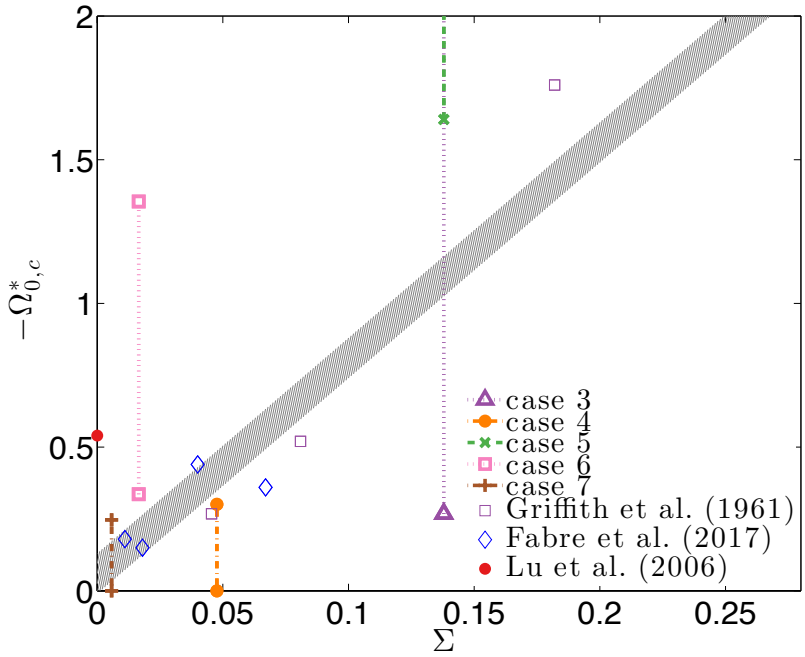

Fig. 6 – Critical value of the vorticity-to-radius ratio, $-\Omega^*_{0,c} = (\omega/r)_0$, for present and literature results. Grey area corresponds to equation 15, proposed byFabre and Figueroa-Espinoza (2014).

depicts the cross sectional bubble shape, streamlines and upstream velocity distribution with the bubble as the moving reference frame, for four cases: case 5 with imposed flow of $Re_{SL} = 10$ and $Re_{SL} = 1$, and case 6 with imposed flow of $Re_{SL} = 10$ and $Re_{SL} = -10$, respectively. There, it can be seen that the wake depends on the tail shape: the convex tail case (case 5, $Re_{SL} = 1$, figure 7b) shows a fairly small wake, whereas that of case 6, $Re_{SL} = 10$ (figure 7c), which has a pronounce concave tail, is the largest. Araújo et al. (2012) studied this characteristic for Taylor bubbles in vertical pipes of stagnant liquid. In order to predict if the bubble tail is convex or concave, the authors proposed a correlation based on data fitting that matched well the present code's results (see figure 6-13 of Lizarraga-García (2016)). For Taylor bubbles in pipes with imposed flow, Lu and Prosperetti (2009) studied the bubble tail shape based on physical phenomena. They proposed an approximate criterion for the bubble tail to be convex by observing that surface tension should be large enough to overcome the stagnant pressure below itself. As the latter can be approximated by the dynamic pressure, the following *Weber* number is obtained:

$$We = \frac{\rho_L (v_{TB} - v_{SL})^2 d}{\sigma} = Eo(Fr_{TB} - Fr_{SL})^2. \quad [16]$$

On the one hand, for low We, the surface tension force is higher than the stagnant pressure force and the tail is convex to the liquid. On the other hand, when We is high, the stagnant pressure on the tail is high enough so that the tail is concave to the liquid. Based on their simulations, Lu and Prosperetti (2009) established the criterion at $We_c \approx 5$.

Figure 8 depicts cases 5 and 6 vertical pipe bubble tails for different upward and downward flows, respectively. In case 5 (figure 8a), as We increases, the tail shape transitions from convex to concave. In case 6 (figure 8b), the bubble tail is concave for all flows, but its concavity is again related with We. For the cases simulated, figure 9 shows the distribution of bubble tail shapes in the Eo-We diagram, where c denotes *convexity* and nc denotes *nonconvexity* or *concavity*. The criteria of Lu and Prosperetti (2009) and Lizarraga-García (2016) are also included, where the later just added a We_c transition region where the tail was approximately flat and thus difficult to classify. It can be observed that bubble tail shapes

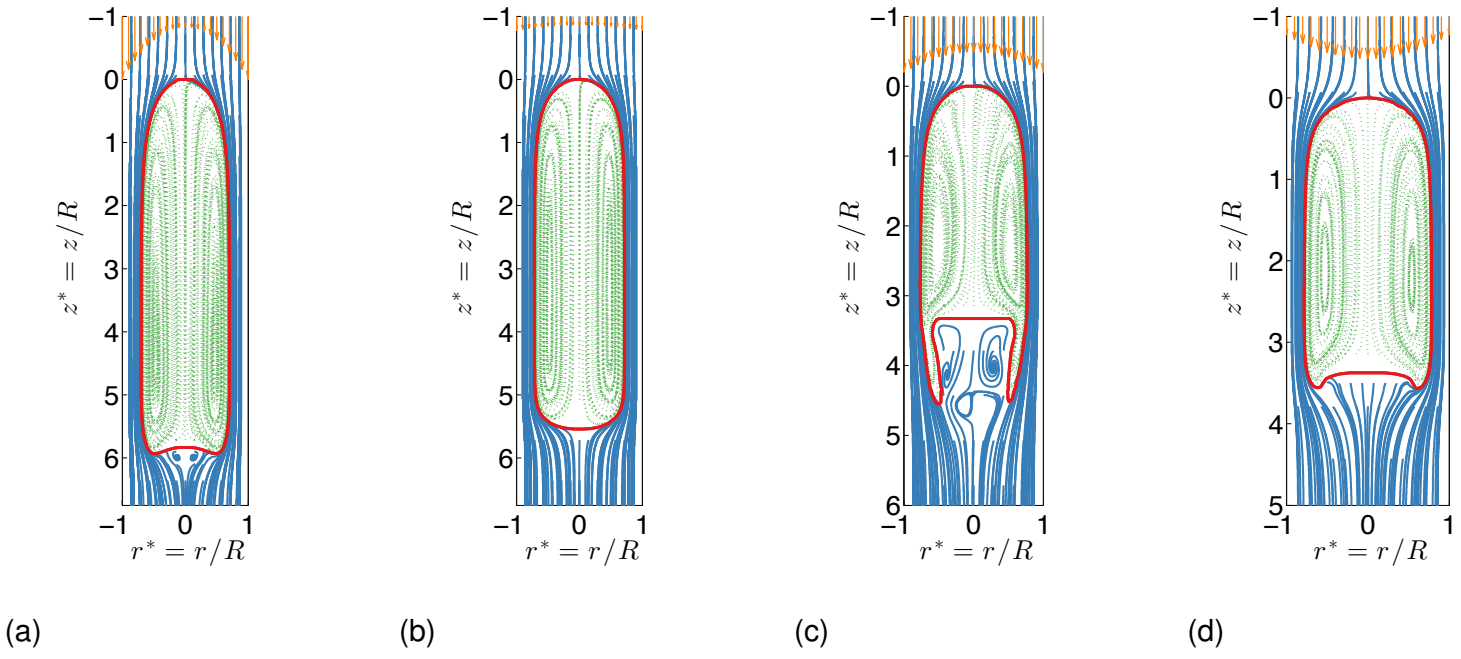

Fig. 7 – Cross sectional Taylor bubble shape, streamlines and upstream velocity distribution for case 5 with imposed flow of $Re_{SL} = 10$ (a) and $Re_{SL} = 1$ (b), and case 6 with imposed flow of $Re_{SL} = 10$ (c) and $Re_{SL} = -10$ (d).

are generally well predicted by the We defined in equation 16. When $We > 5$, every simulated tail is concave. When $We < 1$, every simulated tail but one is convex. In the transition region $1 < We < 5$, the two cases simulated are slightly concave. The one case that does not follow this criterion is the case 3 upward flow. Case 3 represents a very high viscosity liquid (figure 1) where viscous effects may have an effect not captured by equation 16. Nevertheless, based on the results presented here, we think that We of equation 16 can be a good indicator of bubble tail shape.

Inclined pipes. Inclined pipe simulations are performed for cases 5, 6, and 7, including upward and downward flows for $\theta = 45°$ and $5°$ (table 3). In order to analyze the impact of pipe inclination angle on C_0, figure 10 shows those simulated C_0 values compared to the simulated C_0 results obtained for the corresponding vertical pipe cases, $\theta = 90°$, with the same imposed flow, Fr_{SL}.

Figure 10a depicts the cases for $\theta = 45°$, where it can be seen that $C_{0,45°}$ values are significantly lower than $C_{0,90°}$ ones. This is explained by the bubble tip migration toward the pipe wall due to lateral buoyancy in an inclined pipe. In that location, the absolute liquid velocity value is lower than in the pipe axis, thus reducing the liquid flow effect on the bubble velocity. This behavior can be seen in figures 11 to 13, where the Taylor bubble shape dependence on inclination angle is shown for various imposed flows. Furthermore, there are two outliers in figure 10 highlighted by red circles. They correspond to the vertical pipe cases with downward flow where the bubble becomes asymmetric, as shown in figures 12d and 13c. There, the bubble shape and tip location do not change significantly with respect to the vertical case, thus their C_0 values are comparable. Without those outliers, the average of $C_{0,45°}$ results is 31% lower than that of $C_{0,90°}$ ones.

Figure 10b depicts the cases for $\theta = 5°$, where similar behavior is observed: on average, $C_{0,5°}$ is 37% lower than $C_{0,90°}$ for those cases where the bubble remains axisymmetric in the vertical pipe. However, for the two outliers, $C_{0,5°}$ values are actually significantly higher than their $C_{0,90°}$ ones. This result is

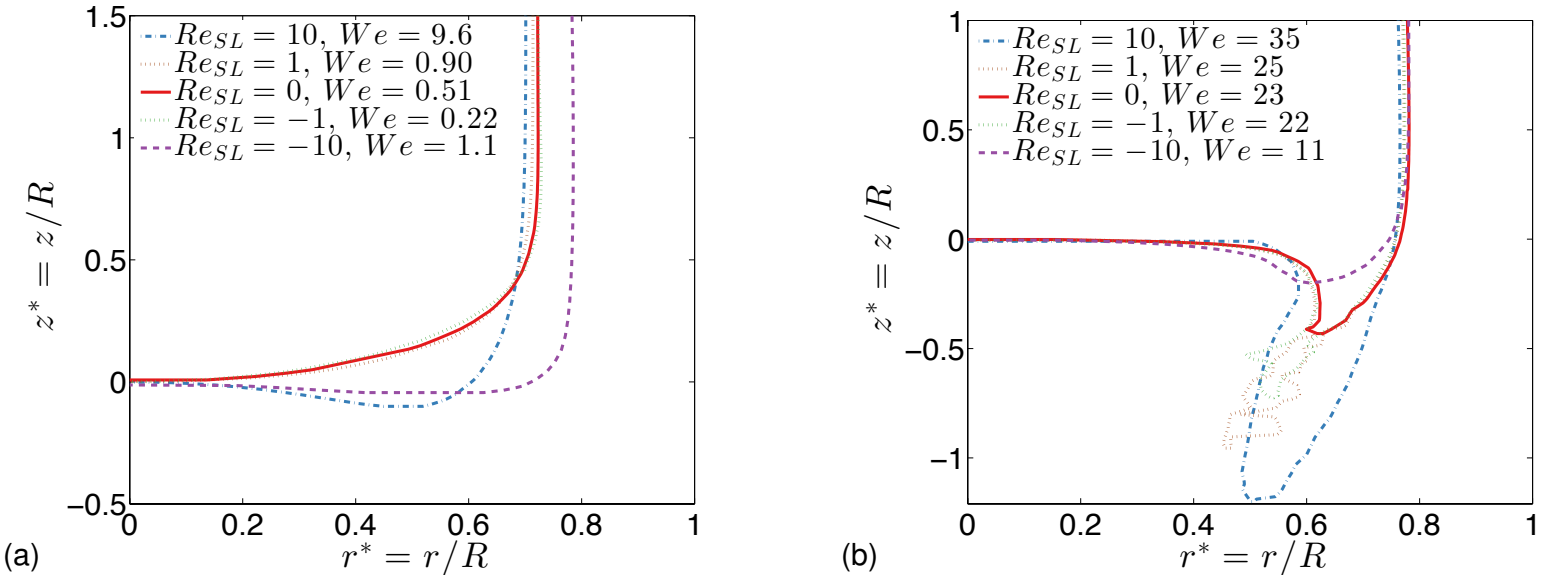

Fig. 8 – Bubble tail shape of case 5 (a) and case 6 (b) in vertical pipes for different upward and downward flows: the tail concavity to the liquid increases with increasing We.

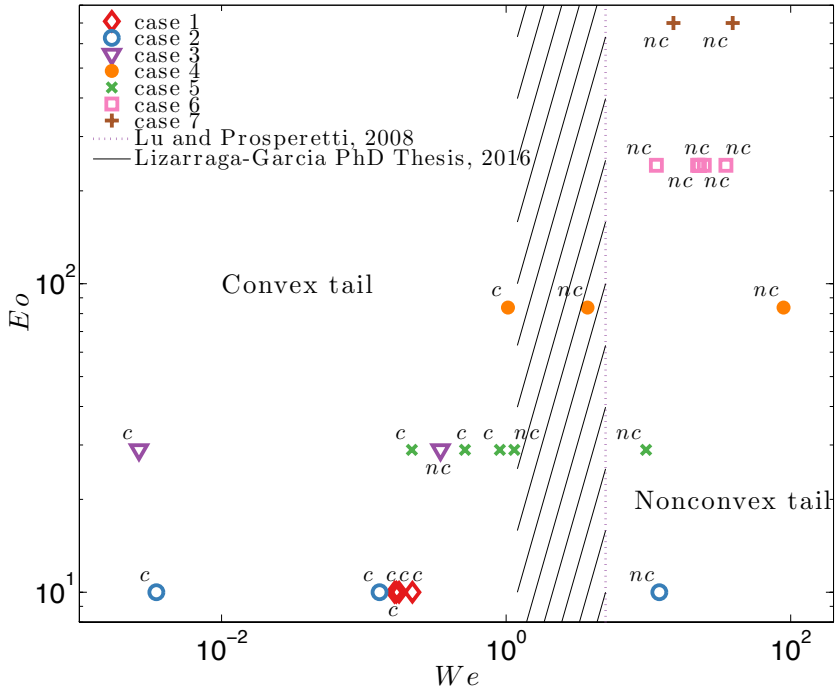

Fig. 9 – Bubble tail shape of present simulations.

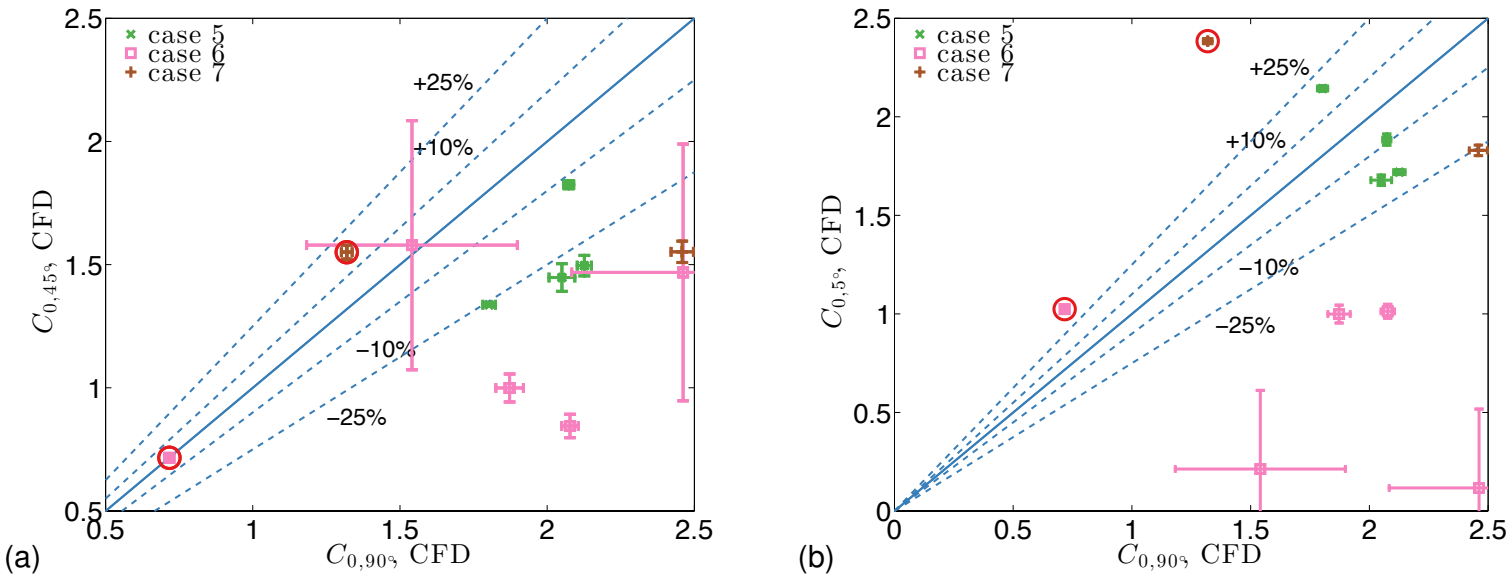

Fig. 10 – Comparison of the simulated C_0 results for $\theta = 45°$ (a) and $\theta = 5°$ (b), respectively, against the simulated C_0 results for vertical pipes, $\theta = 90°$. Red circled cases (○) correspond to asymmetric bubble results in the vertical pipe case.

elucidated by the corresponding bubble shapes. As shown in figures 12d and 13c, while their bubble tip locations remain approximately constant, their bubble shapes change significantly. In the $\theta = 5°$ case, the cross sectional area is reduced considerably, thus reducing its drag when compared with the vertical pipe case which leads to $C_{0,5°} > C_{0,90°}$.

Furthermore, it is also worth noting that the C_0 values of case 5 do not change as significantly as in the other two cases. This behavior can be explained by its lower Eo number (28.7 versus 242 or 700), i.e. its higher surface tension effects. That translates into a lower bubble deformation in the inclined pipe cases where the bubble tip movement toward the pipe wall is reduced. This observation is consistent with the experiments of Bendiksen (1984) at relatively small Eo number ($Eo = 80$), where a C_0 value reduction of just up to 15% was reported for inclined upward flows when compared to the vertical pipe case (see figure 11 of Bendiksen (1984)).

Figures 14 and 15 exhibit the flow structure of case 7 simulations for imposed flows of $Re_{SL} = 1$ and $Re_{SL} = -1$, respectively. In particular, the figures show the cross sectional Taylor bubble shape, streamlines and upstream velocity distribution with the bubble as the reference frame for the three inclination angles analyzed. In the upward flow case, figure 14, the clear transition from the axisymmetric bubble in the vertical pipe case to the asymmetric bubble that has migrated toward the pipe wall in the inclined pipe cases can be observed. In the latter, the majority of the liquid passes the bubble through the bottom part of the pipe where the flow resistance is lower. In the downward flow case, figure 15, the bubble is already asymmetric in the vertical pipe simulation, and its shape and streamlines are comparable with the $\theta = 45°$ case's. Finally, it is worth noting the different flow structure of case $\theta = 5°$, figure 15c, with respect to the others depicted in detail. In this case, the bubble is moving downward, and the upstream velocity distribution with the bubble as the reference frame shows a recirculation: in the pipe center, the liquid moves downward, whereas in the section close to the pipe wall, it moves upward. This creates a vortex in the bottom part of the pipe while the bubble passes.

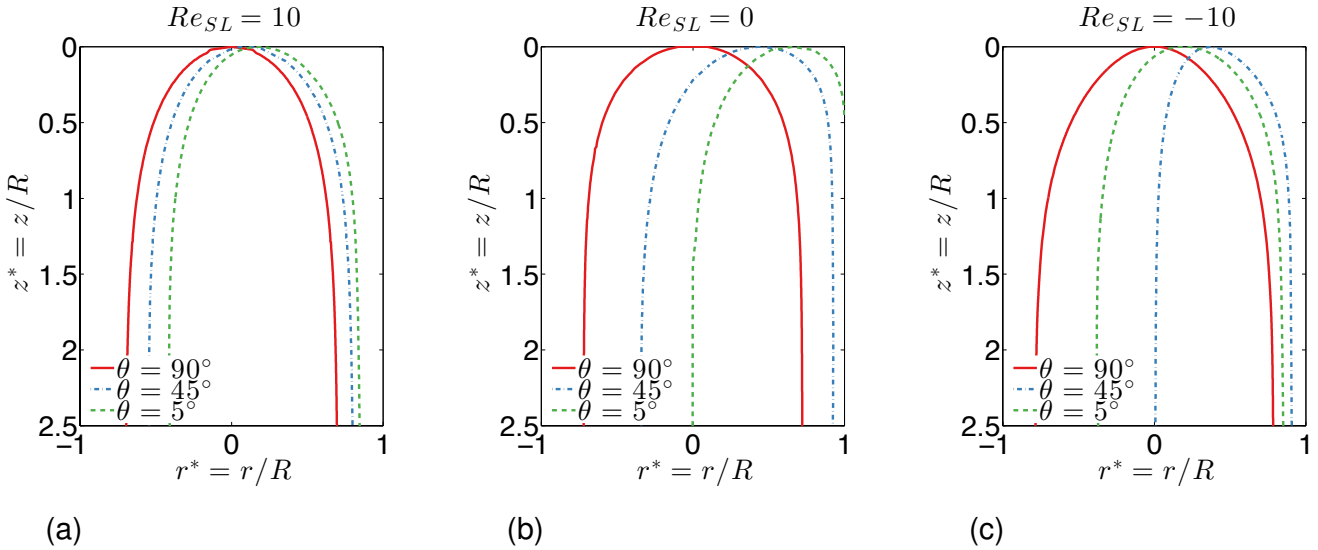

Fig. 11 – Case 5 Taylor bubble shape dependence on inclination angle for imposed flow of $Re_{SL} = 10$ (a), $Re_{SL} = 0$ (b), and $Re_{SL} = -10$ (c).

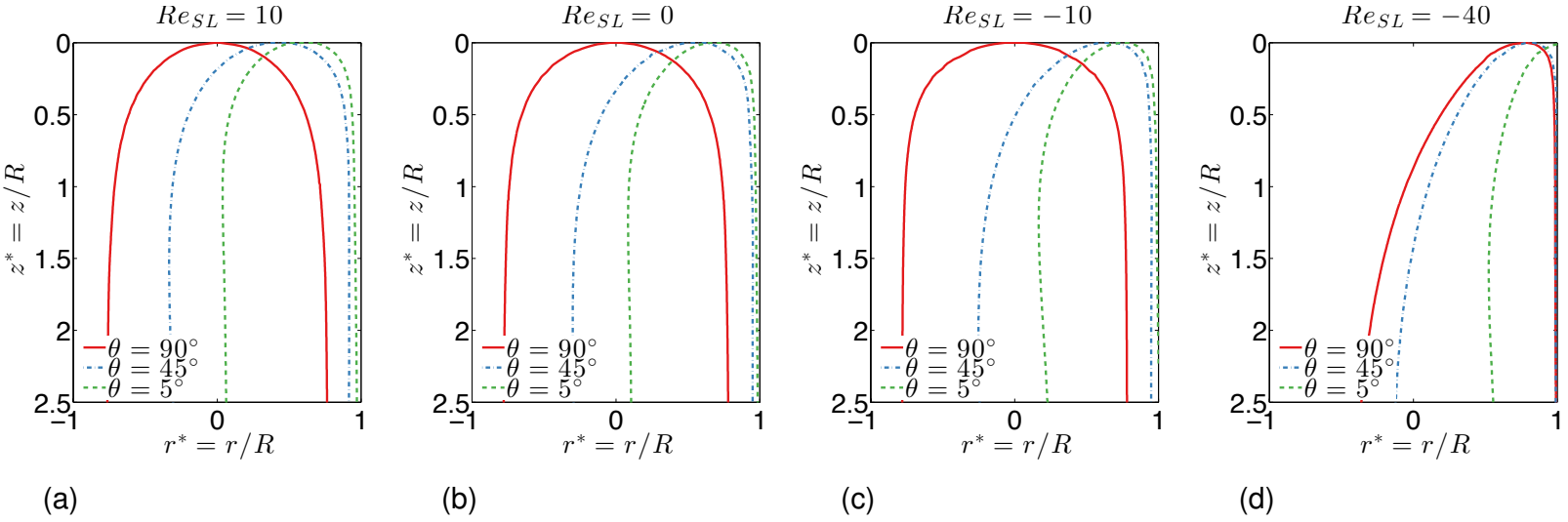

Fig. 12 – Case 6 Taylor bubble shape dependence on inclination angle for imposed flow of $Re_{SL} = 10$ (a), $Re_{SL} = 0$ (b), $Re_{SL} = -10$ (c), and $Re_{SL} = -40$ (d).

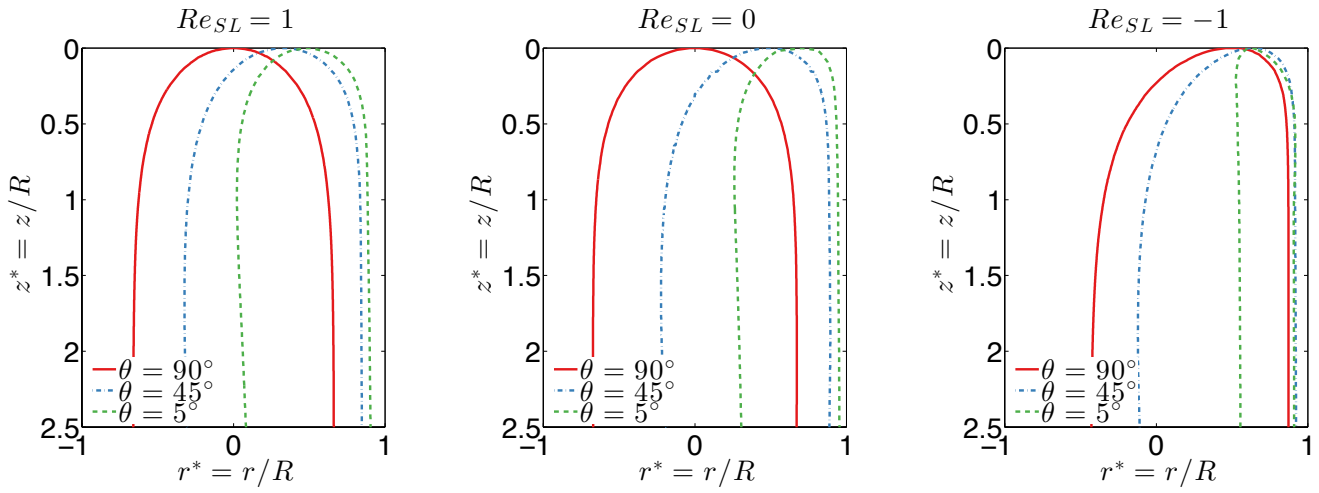

Fig. 13 – Case 7 Taylor bubble shape dependence on inclination angle for imposed flow of $Re_{SL} = 1$ (a), $Re_{SL} = 0$ (b), and $Re_{SL} = -1$ (c).

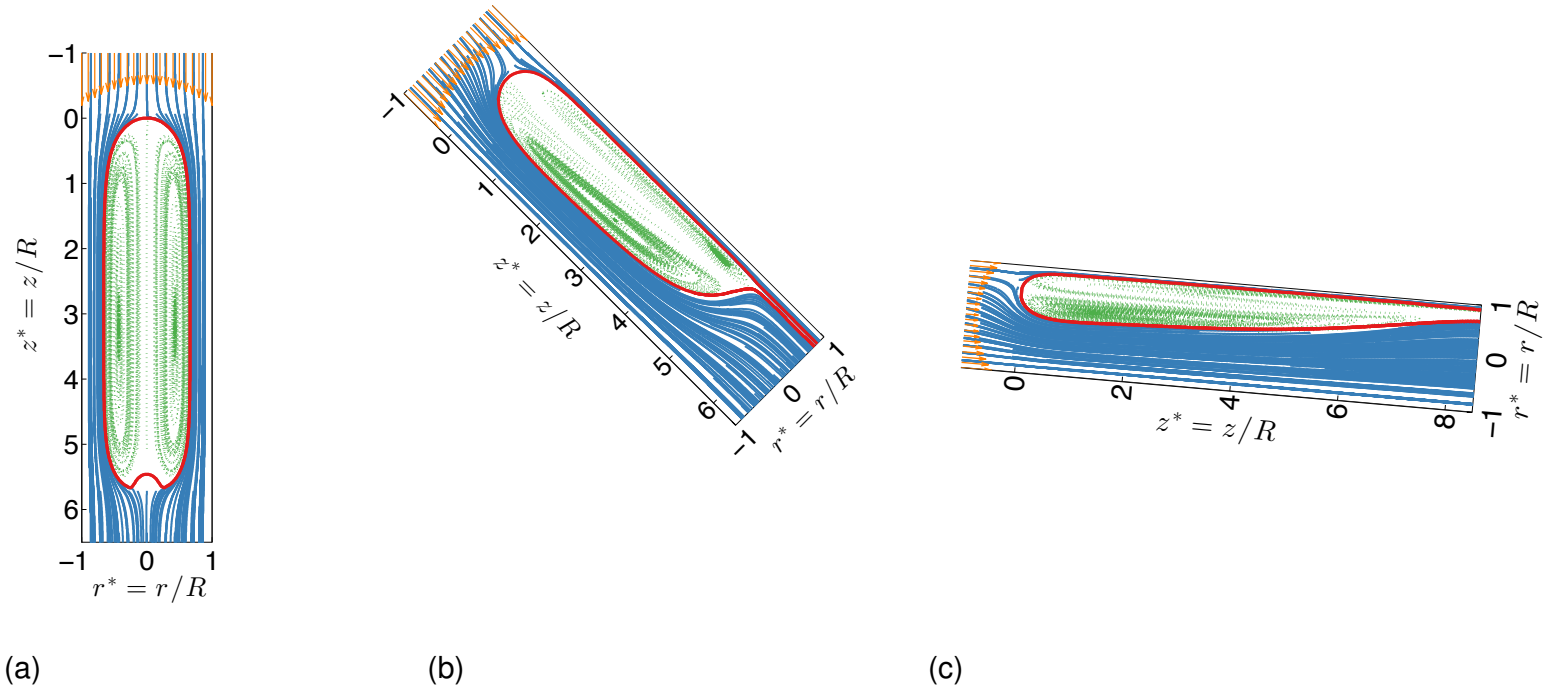

Fig. 14 – Cross sectional Taylor bubble shape, streamlines and upstream velocity distribution for case 7 with imposed flow of $Re_{SL} = 1$ for $\theta = 90°$ (a), $\theta = 45°$ (b), and $\theta = 5°$ (c).

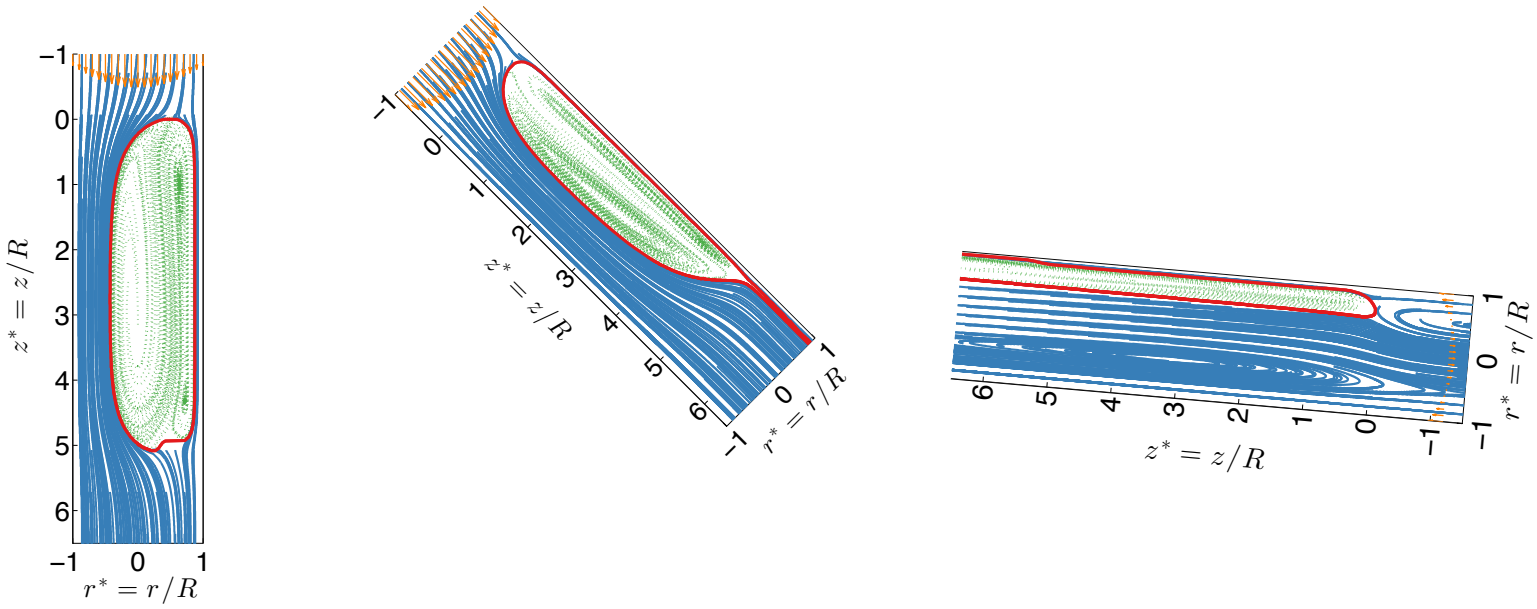

(a) (b) (c)

Fig. 15 – Cross sectional Taylor bubble shape, streamlines and upstream velocity distribution for case 7 with imposed flow of $Re_{SL} = -1$ for $\theta = 90°$ (a), $\theta = 45°$ (b), and $\theta = 5°$ (c).

Conclusions

In this work, we studied the behavior of Taylor bubbles in vertical and inclined pipes with upward and downward flow through 3D CFD simulations that covered a wide range of fluid properties, and pipe diameters and inclination angles ($Eo \in [10, 700]$, $Mo \in [1 \cdot 10^{-6}, 5 \cdot 10^{3}]$, $Re_{SL} \in [-40, 10]$, $\theta \in [5°, 90°]$). The main objective was to analyze the effect of those parameters on the distribution parameter, C_0. The latter is critical to predict the Taylor bubble velocity that strongly affects the pressure gradient and liquid holdup prediction of mechanistic models (Lizarraga-García, 2016), and has been scarcely studied in the literature for vertical downward flows, and also upward and downward flows in inclined pipes. For bubbles in vertical upward flows, C_0 is successfully compared with an existing model. However, it was shown numerically that the asymmetric nature of all inclined slug flows and some vertical downward slug flows where the bubble tip does not occupy the pipe axis altered significantly the C_0 values when compared to their respective symmetric vertical upward flow ones. Further work is required to predict the critical downward flow in vertical pipes at which the bubble becomes asymmetric and the viscosity influence on that phenomenon, as published literature has focused on fluids with lower viscosity than those more often found in oil and gas systems. Finally, pipe inclination angle was shown to have a significant impact on C_0, for which no predictive model currently exists for the fluids studied in this manuscript.

Nomenclature

$AAR =$ absolute average relative error
$AMG =$ Algebraic Multigrid
$CFD =$ Computational Fluid Dynamics
$DNS =$ Direct Numerical Simulation
$GMRES =$ Generalized Minimum Residual method
$HLPA =$ Hybrid Linear/Parabolic Approximation
$IST =$ Immersed Surfaces Technology
$MPI =$ Message Passing Interface
$LS =$ Level Set
$PETSc =$ Portable, Extensible Toolkit for Scientific Computation
$SIMPLEC =$ Semi-Implicit Method for Pressure Linked Equations-Consistent
$SIP =$ Strongly Implicit Procedure
$VOF =$ Volume of Fluid
$WENO =$ Weighted Essentially Non-Oscillatory
$Ca =$ *capillary* number. $\mu_L v_{SL}/\sigma$
$Eo =$ *Eötvös* number. $Eo = \rho_L g d^2/\sigma$
$Fr =$ *Froude* number. $Fr = v/\sqrt{gd}$
$Mo =$ *Morton* number. $Mo = g\mu_L^4/\rho_L\sigma^3$
$N_f =$ *inverse viscosity* number. $N_f = (Eo^3/Mo)^{1/4}$
$Re =$ *Reynolds* number. $Re = \rho_L v d/\mu_L$
$\Sigma =$ inverse *Eötvös* number. $\Sigma = 4\sigma/\rho_L g d^2 = 4/Eo$
$We =$ *Weber* number. $We = (\rho_L(v_{TB} - v_{SL})^2 d)/\sigma = Eo(Fr_{TB} - Fr_{SL})^2$
$C_0 =$ distribution parameter
$d =$ pipe diameter
$g =$ gravitational acceleration
$R^2 =$ coefficient of determination
$v_d =$ drift velocity
$v_m =$ mixture velocity. $v_m = v_{SL} + vSg$
$v_{Sg} =$ gas superficial velocity
$v_{SL} =$ liquid superficial velocity
$v_{TB} =$ Taylor bubble velocity
$_g =$ gas phase (subscript)
$_L =$ liquid phase (subscript)
$_{TB} =$ Taylor bubble (subscript)
$\alpha =$ void fraction
$\eta =$ Kolmogorov scale
$\theta =$ pipe inclination with respect to the horizontal
$\mu =$ viscosity
$\rho =$ density

$\sigma =$ standard error

$\sigma =$ surface tension

$-\Omega_0 =$ *vorticity-to-radius ratio* . $-\Omega_0 = (\omega/r)_0$

Acknowledgements

This work was performed as part of Enrique Lizarraga-Garcia's Ph.D. thesis at MIT, and was sponsored by the MIT-Kuwait Center for Natural Resources and the Environment. Enrique Lizarraga-Garcia is also thankful to the "Caja Madrid" Foundation for his postgraduate fellowship. The authors would like to express their gratitude to Dr. Djamel Lakehal, Dr. Chidu Narayanan and Mr. Daniel Caviezel from ASCOMP for their support with the code. This research used the computational resources of the Oak Ridge Leadership Computing Facility at the Oak Ridge National Laboratory, which is supported by the Office of Science of the U.S. Department of Energy under Contract No. DE-AC05-00OR22725. Declaration of Interests. The authors report no conflict of interest.

Numerical database results

Table 6 – Numerical database results

Case	Eo	Mo	N_f	θ (°)	Re_{SL}	Fr_{SL}	Fr_{TB}	Re_{TB}	C_0
1	10	$1{\cdot}10^{-6}$	178	90	0	0	0.130	23.1	-
1	10	$1{\cdot}10^{-6}$	178	90	1	0.00562	0.139	24.7	1.5±0.2
1	10	$1{\cdot}10^{-6}$	178	90	10	0.0562	0.204	36.4	1.32±0.03
1	10	$1{\cdot}10^{-6}$	178	90	-1	-0.00562	0.122	21.8	1.4±0.2
2	10	$7.07{\cdot}10^{-2}$	10.9	90	0	0	0.0186	0.203	-
2	10	$7.07{\cdot}10^{-2}$	10.9	90	1	0.0917	0.205	2.24	2.04±0.02
2	10	$7.07{\cdot}10^{-2}$	10.9	90	10	0.917	2.01	21.9	2.17±0.02
3	28.9	$5{\cdot}10^{3}$	1.48	90	0	0	0.00953	0.0141	-
3	28.9	$5{\cdot}10^{3}$	1.48	90	0.1	0.0674	0.177	0.262	2.48±0.02
3	28.9	$5{\cdot}10^{3}$	1.48	90	-0.1	-0.0674	-0.124	-0.184	1.98±0.01
4	83.7	18.8	13	90	0	0	0.111	1.47	-
4	83.7	18.8	13	90	1	0.0753	0.287	3.80	2.33±0.03
4	83.7	18.8	13	90	10	0.753	1.79	23.7	2.22±0.02
4	83.7	18.8	13	90	-1	-0.0753	0.00929	0.123	1.35±0.01
5	28.9	$7.07{\cdot}10^{-2}$	24.2	90	0	0	0.133	3.22	-
5	28.9	$7.07{\cdot}10^{-2}$	24.2	90	1	0.0413	0.218	5.27	2.05±0.04
5	28.9	$7.07{\cdot}10^{-2}$	24.2	90	10	0.413	0.990	24.0	2.07±0.02
5	28.9	$7.07{\cdot}10^{-2}$	24.2	90	-1	-0.0413	0.0454	1.10	2.12±0.02
5	28.9	$7.07{\cdot}10^{-2}$	24.2	90	-10	-0.413	-0.612	-14.8	1.80±0.02
5	28.9	$7.07{\cdot}10^{-2}$	24.2	45	0	0	0.200	4.84	-
5	28.9	$7.07{\cdot}10^{-2}$	24.2	45	1	0.0413	0.260	6.30	1.45±0.06
5	28.9	$7.07{\cdot}10^{-2}$	24.2	45	10	0.413	0.955	23.1	1.82±0.02
5	28.9	$7.07{\cdot}10^{-2}$	24.2	45	-1	-0.0413	0.138	3.35	1.50±0.04
5	28.9	$7.07{\cdot}10^{-2}$	24.2	45	-10	-0.413	-0.353	-8.53	1.34±0.01
5	28.9	$7.07{\cdot}10^{-2}$	24.2	5	0	0	0.0706	1.71	-
5	28.9	$7.07{\cdot}10^{-2}$	24.2	5	1	0.0413	0.140	3.39	1.68±0.03
5	28.9	$7.07{\cdot}10^{-2}$	24.2	5	10	0.413	0.850	20.6	1.88±0.01
5	28.9	$7.07{\cdot}10^{-2}$	24.2	5	-1	-0.0413	-0.000470	-0.0114	1.72±0.01
5	28.9	$7.07{\cdot}10^{-2}$	24.2	5	-10	-0.413	-0.816	-19.7	2.14±0.01
6	242	$7.07{\cdot}10^{-2}$	119	90	0	0	0.307	36.6	-
6	242	$7.07{\cdot}10^{-2}$	119	90	1	0.00840	0.328	39.0	2.5±0.4
6	242	$7.07{\cdot}10^{-2}$	119	90	10	0.0840	0.465	55.3	1.87±0.05
6	242	$7.07{\cdot}10^{-2}$	119	90	-1	-0.00840	0.294	35.0	1.5±0.4
6	242	$7.07{\cdot}10^{-2}$	119	90	-10	-0.0840	0.133	15.8	2.08±0.03
6	242	$7.07{\cdot}10^{-2}$	119	90	-40	-0.339	0.0646	7.69	0.72±0.01
6	242	$7.07{\cdot}10^{-2}$	119	45	0	0	0.432	51.4	-
6	242	$7.07{\cdot}10^{-2}$	119	45	1	0.00840	0.444	52.8	1.5±0.5
6	242	$7.07{\cdot}10^{-2}$	119	45	10	0.0840	0.516	61.3	1.00±0.06
6	242	$7.07{\cdot}10^{-2}$	119	45	-1	-0.00840	0.418	49.8	1.6±0.5
6	242	$7.07{\cdot}10^{-2}$	119	45	-10	-0.0840	0.361	42.9	0.85±0.05
6	242	$7.07{\cdot}10^{-2}$	119	45	-40	-0.339	0.189	22.5	0.72±0.01
6	242	$7.07{\cdot}10^{-2}$	119	5	0	0	0.336	40.0	-
6	242	$7.07{\cdot}10^{-2}$	119	5	1	0.00840	0.337	40.1	0.1±0.4
6	242	$7.07{\cdot}10^{-2}$	119	5	10	0.0840	0.420	50.0	1.00±0.05
6	242	$7.07{\cdot}10^{-2}$	119	5	-1	-0.00840	0.334	39.8	0.2±0.4
6	242	$7.07{\cdot}10^{-2}$	119	5	-10	-0.0840	0.251	29.8	1.01±0.04
6	242	$7.07{\cdot}10^{-2}$	119	5	-40	-0.339	-0.0108	-1.29	1.02±0.01
7	700	$5{\cdot}10^{3}$	16.2	90	0	0	0.146	2.37	-
7	700	$5{\cdot}10^{3}$	16.2	90	1	0.0618	0.298	4.83	2.46±0.04
7	700	$5{\cdot}10^{3}$	16.2	90	-1	-0.0618	0.0649	1.05	1.32±0.02
7	700	$5{\cdot}10^{3}$	16.2	45	0	0	0.215	3.48	-
7	700	$5{\cdot}10^{3}$	16.2	45	1	0.0618	0.311	5.03	1.55±0.04
7	700	$5{\cdot}10^{3}$	16.2	45	-1	-0.0618	0.119	1.93	1.55±0.03
7	700	$5{\cdot}10^{3}$	16.2	5	0	0	0.0985	1.59	-
7	700	$5{\cdot}10^{3}$	16.2	5	1	0.0618	0.212	3.42	1.83±0.03
7	700	$5{\cdot}10^{3}$	16.2	5	-1	-0.0618	-0.0488	-0.790	2.38±0.01

References

Ansari, A. M., Sylvester, N. D., Sarica, C., Shoham, O., and Brill, J. P. (1994). A comprehensive mechanistic model for upward two-phase flow in wellbores. *SPE Production & Facilities*, 9(2):143–151.

Araújo, J. D. P., Miranda, J. M., Pinto, A. M. F. R., and Campos, J. B. L. M. (2012). Wide-ranging survey on the laminar flow of individual Taylor bubbles rising through stagnant Newtonian liquids. *International Journal of Multiphase Flow*, 43:131–148.

Balay, S., Gropp, W. D., McInnes, L. C., and Smith, B. F. (1997). Efficient management of parallelism in object-oriented numerical software libraries. In *Modern Software Tools for Scientific Computing*, pages 163–202. Springer.

Beckermann, C., Diepers, H.-J., Steinbach, I., Karma, A., and Tong, X. (1999). Modeling melt convection in phase-field simulations of solidification. *Journal of Computational Physics*, 154(2):468–496.

Bendiksen, K. H. (1984). An experimental investigation of the motion of long bubbles in inclined tubes. *International Journal of Multiphase Flow*, 10(4):467–483.

Bendiksen, K. H. (1985). On the motion of long bubbles in vertical tubes. *International Journal of Multiphase Flow*, 11(6):797–812.

Bendiksen, K. H., Malnes, D., and Nydal, O. J. (1996). On the modelling of slug flow. *Chemical Engineering Communications*, 141(1):71–102.

Brill, J. P. and Mukherjee, H. (1999). Multiphase flow in wells. *Monograph Vol. 17, SPE Henry L. Dogorty Series*.

British Petroleum (2011). Heavy Oil vs. Light Oil. Technical report, BP.

Chung, M.-H. (2001). A level set approach for computing solutions to inviscid compressible flow with moving solid boundary using fixed cartesian grids. *International Journal for Numerical Methods in Fluids*, 36(4):373–389.

Collins, R., Moraes, F. F. D., Davidson, J. F., and Harrison, D. (1978). The motion of a large gas bubble rising through liquid flowing in a tube. *Journal of Fluid Mechanics*, 89(3):497–514.

de Azevedo, M. B., Faccini, J. L., and Su, J. (2020). Experimental study of single Taylor bubbles rising in vertical and slightly deviated circular tubes. *Experimental Thermal and Fluid Science*, 116:110109.

Doormaal, J. P. V. and Raithby, G. D. (1984). Enhancements of the SIMPLE method for predicting incompressible fluid flows. *Numerical Heat Transfer*, 7(2):147–163.

Fabre, J. and Figueroa-Espinoza, B. (2014). Taylor bubble rising in a vertical pipe against laminar or turbulent downward flow: symmetric to asymmetric shape transition. *Journal of Fluid Mechanics*, 755:485–502.

Fabre, J. and Liné, A. (1992). Modeling of two-phase slug flow. *Annual Review of Fluid Mechanics*, 24(1):21–46.

Falgout, R. D., Jones, J. E., and Yang, U. M. (2006). The design and implementation of hypre, a library of parallel high performance preconditioners. In *Numerical Solution of Partial Differential Equations on Parallel Computers*, pages 267–294. Springer.

Fershtman, A., Babin, V., Barnea, D., and Shemer, L. (2017). On shapes and motion of an elongated bubble in downward liquid pipe flow. *Physics of Fluids*, 29(11):112103.

Figueroa-Espinoza, B. and Fabre, J. (2011). Taylor bubble moving in a flowing liquid in vertical channel: transition from symmetric to asymmetric shape. *Journal of Fluid Mechanics*, 679:432–454.

Fréchou, D. (1986). Etude de l'écoulement ascendant à trois fluides en conduite verticale. *These Inst Natl Polythech, Toulouse, France*.

Gomez, L. E., Shoham, O., Schmidt, Z., Chokshi, R. N., and Northug, T. (2000). Unified mechanistic model for steady-state two-phase flow: horizontal to vertical upward flow. *SPE Journal*, 5(3):339–350.

Griffith, P. and Wallis, G. B. (1961). Two-phase slug flow. *Journal of Heat Transfer*, 83(3):307–318.

Ha-Ngoc, H. and Fabre, J. (2004). Test-case No 29b: The velocity and shape of 2D long bubbles in inclined channels or in vertical tubes (PA, PN) Part II: in a flowing liquid. *Multiphase Science and Technology*, 16(1-3):191–206.

Hua, J., Langsholt, M., and Lawrence, C. (2012). Numerical simulation of single elongated bubble propagation in inclined pipes. *Progress in Computational Fluid Dynamics, an International Journal*, 12(2-3):131–139.

Labois, M., Panyasantisuk, J., Höhne, T., Kliem, S., and Lakehal, D. (2010). On the prediction of boron dilution using the CMFD code TRANSAT: the ROCOM test case. In *Proc. CFD4NRS 4. OECD-NEA, Washington, USA*.

Lakehal, D., Meier, M., and Fulgosi, M. (2002). Interface tracking towards the direct simulation of heat and mass transfer in multiphase flows. *International Journal of Heat and Fluid Flow*, 23(3):242 – 257.

Liu, H., Vandu, C. O., and Krishna, R. (2005). Hydrodynamics of Taylor flow in vertical capillaries: flow regimes, bubble rise velocity, liquid slug length, and pressure drop. *Industrial & Engineering Chemistry Research*, 44(14):4884–4897.

Lizarraga-García, E. (2016). *A study of Taylor bubbles in vertical and inclined slug flow using multiphase CFD with level set*. PhD thesis, Massachusetts Institute of Technology.

Lizarraga-Garcia, E., Buongiorno, J., Al-Safran, E., and Lakehal, D. (2015). Development of a new CFD-based unified closure relation for Taylor bubble velocity in two-phase slug flow in pipes. In *17th International Conference on Multiphase Production Technology, Cannes, France*, pages 93–107. BHR Group.

Lizarraga-Garcia, E., Buongiorno, J., Al-Safran, E., and Lakehal, D. (2017). A broadly-applicable unified closure relation for Taylor bubble rise velocity in pipes with stagnant liquid. *International Journal of Multiphase Flow*, 89:345–358.

Lizarraga-Garcia, E., Buongiorno, J., and Bucci, M. (2016). An analytical film drainage model and breakup criterion for Taylor bubbles in slug flow in inclined round pipes. *International Journal of Multiphase Flow*, 84:46–53.

Lu, X. and Prosperetti, A. (2006). Axial stability of Taylor bubbles. *Journal of Fluid Mechanics*, 568:173–192.

Lu, X. and Prosperetti, A. (2009). A numerical study of Taylor bubbles. *Industrial & Engineering Chemistry Research*, 48(1):242–252.

Mao, Z.-S. and Dukler, A. E. (1990). The motion of Taylor bubbles in vertical tubes–I. A numerical simulation for the shape and rise velocity of Taylor bubbles in stagnant and flowing liquid. *Journal of Computational Physics*, 91(1):132 – 160.

Mao, Z.-S. and Dukler, A. E. (1991). The motion of Taylor bubbles in vertical tubes–II. Experimental data and simulations for laminar and turbulent flow. *Chemical Engineering Science*, 46(8):2055 – 2064.

Martin, C. S. (1976). Vertically downward two-phase slug flow. *Journal of Fluids Engineering*, 98(4):715–722.

Massoud, E. Z. (2019). *The rise of Taylor bubbles in vertical and inclined pipes*. PhD thesis, University of Strathclyde.

Mitchell, T. (2019). *Development of a multiphase lattice Boltzmann model for high-density and viscosity ratio flows in unconventional gas wells*. PhD thesis, The University of Queensland.

Nicklin, D. J., Wilkes, J. O., and Davidson, J. F. (1962). Two-phase flow in vertical tubes. *Trans. Inst. Chem. Eng*, 40(1):61–68.

Orell, A. and Rembrand, R. (1986). A model for gas-liquid slug flow in a vertical tube. *Industrial & Engineering Chemistry Fundamentals*, 25(2):196–206.

Osher, S. and Sethian, J. A. (1988). Fronts propagating with curvature-dependent speed: algorithms based on Hamilton-Jacobi formulations. *Journal of Computational Physics*, 79(1):12–49.

Petalas, N. and Aziz, K. (2000). A mechanistic model for multiphase flow in pipes. *Journal of Canadian Petroleum Technology*, 39(6):43–55.

Polonsky, S., Shemer, L., and Barnea, D. (1999). The relation between the Taylor bubble motion and the velocity field ahead of it. *International Journal of Multiphase Flow*, 25(6):957–975.

R-cycle (2016). Personal communication.

Rattner, A. S. and Garimella, S. (2015). Vertical upward intermediate scale Taylor flow: Experiments and kinematic closure. *International Journal of Multiphase Flow*, 75:107–123.

Roumazeilles, P. M., Yang, J., Sarica, C., Chen, X., Wilson, J., and Brill, J. P. (1996). An experimental study on downward slug flow in inclined pipes. *SPE Production & Facilities*, 11(03):173–178.

Saad, Y. and Schultz, M. H. (1986). GMRES: A generalized minimal residual algorithm for solving nonsymmetric linear systems. *SIAM Journal on Scientific and Statistical Computing*, 7(3):856–869.

Stone, H. L. (1968). Iterative solution of implicit approximations of multidimensional partial differential equations. *SIAM Journal on Numerical Analysis*, 5(3):530–558.

Sussman, M., Smereka, P., and Osher, S. (1994). A level set approach for computing solutions to incompressible two-phase flow. *Journal of Computational Physics*, 114(1):146–159.

Taha, T. and Cui, Z. F. (2006). CFD modelling of slug flow in vertical tubes. *Chemical Engineering Science*, 61(2):676–687.

Taitel, Y. and Barnea, D. (1990). Two-phase slug flow. *Advances in Heat Transfer*, 20:83–132.

Tomiyama, A., Nakahara, Y., and Morita, G. (2001). Rising velocities and shapes of single bubbles in vertical pipes. *International Conference of Multiphase Flow*, pages 1–12.

TransAT® (2014). version 5.1.1. *ASCOMP GmbH, Zurich, Switzerland*.

White, E. T. and Beardmore, R. H. (1962). The velocity of rise of single cylindrical air bubbles through liquids contained in vertical tubes. *Chemical Engineering Science*, 17(5):351–361.

Zhu, J. (1991). A low-diffusive and oscillation-free convection scheme. *Communications in Applied Numerical Methods*, 7(3):225–232.

Zuber, N. and Findlay, J. A. (1965). Average volumetric concentration in two-phase flow systems. *Journal of Heat Transfer*, 87:453–464.